














Electromagnetic dressing of the electron energy spectrum of Au(111) at high momenta

Marius Keunecke ^{1,*}, Marcel Reutzel ^{1,†}, David Schmitt ¹, Alexander Osterkorn ², Tridev A. Mishra ², Christina Möller ¹,
 Wiebke Bennecke ¹, G. S. Matthijs Jansen ¹, Daniel Steil ¹, Salvatore R. Manmana ², Sabine Steil ¹,
 Stefan Kehrein ² and Stefan Mathias ^{1,‡}

¹*I. Physikalisches Institut, Georg-August-Universität Göttingen, Friedrich-Hund-Platz 1, 37077 Göttingen, Germany*

²*Institut für Theoretische Physik, Georg-August-Universität Göttingen, Friedrich-Hund-Platz 1, 37077 Göttingen, Germany*



(Received 28 August 2020; accepted 29 September 2020; published 15 October 2020)

Light-engineering of quantum materials via electromagnetic dressing is considered an on-demand approach for tailoring electronic band dispersions and even inducing topological phase transitions. For probing such dressed bands, photoemission spectroscopy is an ideal tool, and we employ here a novel experiment based on ultrafast photoemission momentum microscopy. Using this setup, we measure the in-plane momentum-dependent intensity fingerprints of the electromagnetically-dressed sidebands from a Au(111) surface for *s*- and *p*-polarized infrared driving. We find that at metal surfaces, due to screening of the driving laser, the contribution from Floquet-Bloch bands is negligible, and the dressed bands are dominated by the laser-assisted photoelectric effect. Also, we find, from calculations, that in contrast to general expectations, *s*-polarized light can dress free-electron states at large photoelectron momenta. Our results show that the dielectric response of the material must carefully be taken into account when using photoemission for the identification of light-engineered electronic band structures.

DOI: [10.1103/PhysRevB.102.161403](https://doi.org/10.1103/PhysRevB.102.161403)

The on-demand femtosecond engineering of quantum materials by time-dependent external perturbations is a promising route for dynamical control of physical and chemical properties [1]. For sufficiently strong external stimuli, the eigenstates of the equilibrium system are renormalized. The material's properties then depend on the crystal potential defined by the periodic arrangement of atoms in real space, and, in addition, on the periodicity and strength of the external stimuli; novel phases of matter can be created as has been reviewed in the context of Floquet engineering [2,3]. A particularly promising perturbation is the periodic electric field of an ultrashort laser pulse that can be used to engineer the energy-, momentum-, and time-dispersive band structure of a material [4–14]. In a stroboscopic photoemission experiment, an intense driving field is used to build up an out-of-equilibrium band structure, while a weak probe field maps its current status [5,7,8].

In such a time- and angle-resolved photoemission spectroscopy (TR-ARPES) experiment, the light-dressed band structure is evident in the formation of so-called Floquet-Bloch bands as sketched in Fig. 1(a). Those Floquet-Bloch bands appear as replicas of the main Bloch band spaced by

the photon energy due to the time periodicity of the driving field. Crucially, for the unambiguous identification of light-induced Floquet-Bloch bands in a two-color photoemission experiment, the laser-assisted photoelectric effect (LAPE) has to be considered in addition [15,16]: the LAPE process creates sidebands of the main photoemission line at the same final state energy as would be expected for the photoexcitation of Floquet-Bloch bands [Fig. 1(b)]. However, while Floquet-Bloch bands represent a coherent modification of the electronic band structure of the material, LAPE is a final state effect, in which the photoemitted electron interacts with the electric field of the driving pulse in front of the surface. In consequence, LAPE does not have the potential to engineer material properties and is basically undesired in the quest of band-structure engineering by light. Still, as both processes terminate at the same photoelectron energy, interference of both processes is expected [17] [Fig. 1(c)], which can be used to amplify the spectral signatures of Floquet-Bloch bands in TR-ARPES [7,17].

In this Rapid Communication, we study the contributions of Floquet-Bloch versus LAPE bands from a Au(111) metal surface throughout the full accessible photoemission horizon, considering thus large in-plane momentum. Our analysis shows that on metal surfaces, the sideband formation is largely determined by LAPE. We further outline that not the impinging electric field strength of the driving light field builds up the sideband intensity, but the macroscopic screening response of the studied material defines the electric field strength available for dressing the electromagnetic energy spectrum, which can be crucially different for Floquet and LAPE that occur within and in front of the crystal, respectively.

*mkeunec@gwdg.de

†marcel.reutzel@phys.uni-goettingen.de

‡smathias@uni-goettingen.de

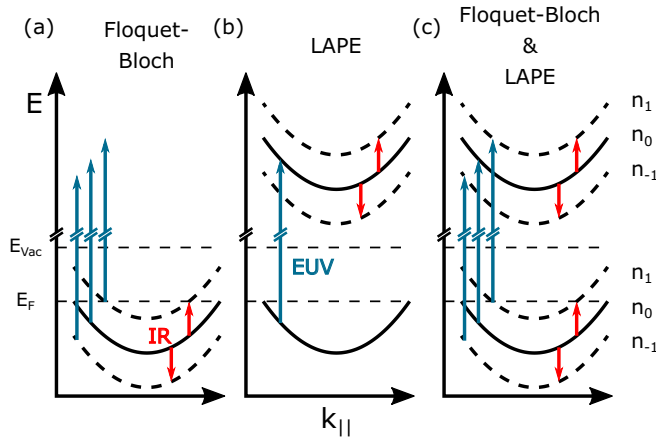


FIG. 1. Schematics for the electromagnetic dressing with IR light of (a) Bloch bands, yielding Floquet-Bloch bands, and (b) quasifree electrons, leading to LAPE. In both scenarios, sidebands ($n_{\pm 1}$, dashed line) of the main photoemission spectral feature (n_0 , solid line) are observed in the photoemission experiment. (c) Both processes terminate at the same final state energy, requiring the consideration of scattering amplitude between both processes.

In Fig. 2, we show exemplary TR-ARPES data obtained on the pristine Au(111) surface, which is driven with an infrared laser pulse at an incidence fluence of 5 mJ/cm^2 (IR, $\hbar\omega = 1.2 \text{ eV}$, nearly p -polarized, $\approx 40 \text{ fs}$). Photoemission is induced by an extreme ultraviolet (EUV) light pulse generated by a table-top high-harmonic generation beamline operated at 1 MHz repetition rate ($\hbar\omega = 26.5 \text{ eV}$, p polarization) [19]. With our novel time-of-flight momentum microscope (ToF-MM) [20], we measure the photoelectron yield as a function of kinetic energy (E_{kin}) and full in-plane momentum (k_x and k_y) [19,21]. The EUV photons map the Fermi level to a kinetic energy of 21.2 eV (photon energy $\hbar\omega = 26.5 \text{ eV}$ minus vacuum level $E_V = 5.3 \text{ eV}$), facilitating the access of in-plane momenta up to $k_{x,y} \approx 2.4 \text{ \AA}^{-1}$, thus covering the full first surface Brillouin zone and parts of the second Brillouin zone of Au(111). Photoelectrons that are detected at higher kinetic energies (corresponding to $E - E_F > 0 \text{ eV}$ in Fig. 2) must have interacted with the EUV probe and the IR driving laser field before their experimental detection. This two-color interaction can be of multiple origin: (i) In real interband transitions, electrons can be excited by the IR pulse into initially unoccupied bands and subsequently photoexcited above the vacuum level with the EUV pulse. (ii) EUV photons might probe the Floquet-Bloch bands of positive photon order that are built up by the intense IR laser field. Finally, (iii) quasifree photoelectrons emitted by the EUV pulse might be dressed by the IR laser field in front of the surface, evident as LAPE. However, for our experimental parameters, we do not map any real unoccupied bands that could be photoexcited via process (i), even so this has been shown for Au(111) when using photon energies in the infrared regime [22,23]. Instead, the photoemission spectral replica features in Fig. 2 can be attributed to first-order sidebands n_1 with the momentum-resolved intensity distribution $I_1(k_{xy}, \theta_k, k_z)$ of the zero-photon-order photoemission spectral feature n_0 ($I_0(k_{xy}, \theta_k, k_z)$). In the following, we discuss the in-plane

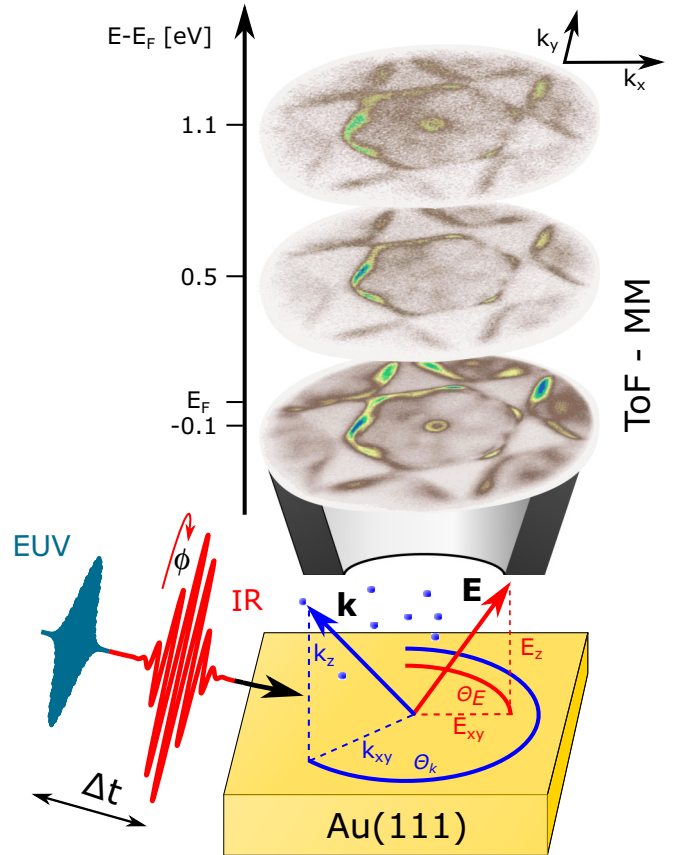


FIG. 2. Time-resolved momentum microscopy experiment. In a stroboscopic experiment, we drive the Au(111) crystal with intense IR laser pulses and probe the instantaneous band structure with EUV light. The momentum microscope provides simultaneous access to the kinetic energy (E_{kin}) and full in-plane momentum-resolved (k_x and k_y) data sets, as illustrated by the three momentum maps at energies $E - E_F$ of 1.1 , 0.5 , and -0.1 eV . The accessible in-plane momentum range is limited by the photoemission horizon that scales with $k_{xy} \propto \sqrt{E_{\text{kin}}}$. The experimental geometry is sketched in the bottom part. The drive and probe laser pulses impinge nearly collinear onto the surface at an angle of 22° from the surface plane. The coordinate frame of the in-plane electric field (E_{xy} , θ_E) and momentum (k_{xy} , θ_k) components is shown in polar coordinates; the out-of-plane components E_z and k_z are normal to the surface. The polarization of the driving light is tuned with a $\lambda/2$ plate and defined by the angle ϕ .

momentum-resolved intensity distributions of these sidebands that are generated by processes (ii) and (iii). Especially, we will focus on the formation of sidebands at large in-plane momenta ($k_{xy} \geq 1 \text{ \AA}^{-1}$), which has to our knowledge not been studied previously.

Before we go into detail of our experimental results, we first calculate the expected momentum fingerprints of the first-order sidebands; their photoemission yield scales with

$$I_1(k_{xy}, \theta_k, k_z) \sim I'_0(k_{xy}, \theta_k, k_z) \times |a_1|^2, \quad (1)$$

where $I'_0(k_{xy}, \theta_k, k_z)$ is the photoemission yield of the undriven system, and $|a_1|^2$ is the sideband amplitude. In early work by Miaja-Avila *et al.* [15,16], sidebands in two-color TR-ARPES experiments have been explained by pure LAPE physics. Only later, Gedik and coworkers [5,7] reasoned that simultaneously

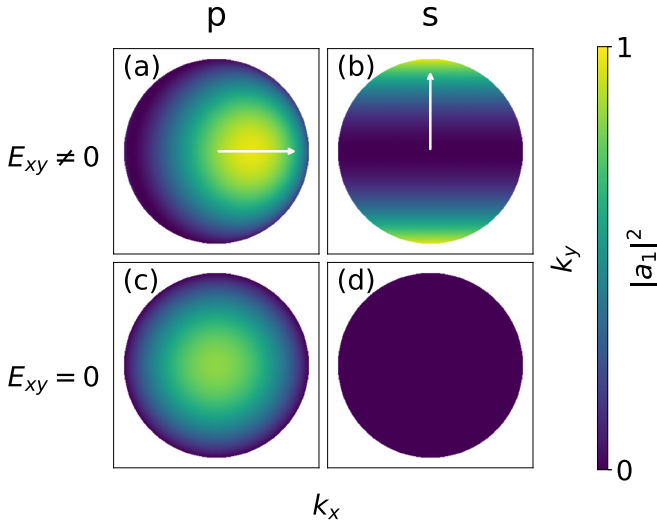


FIG. 3. [(a) and (b)] Calculated in-plane momentum distributions of the LAPE sideband amplitude $|a_1|^2$ after Eq. (3) for p - and s -polarized light impinging along k_x in an oblique angle of incidence; the white arrow indicates the direction of the in-plane electric field component. Sideband yield can be expected for LAPE in both polarizations. [(c) and (d)] If the in-plane electric field components are screened ($E_{xy} = 0$), no sidebands are expected for s -polarized light. In p -polarized driving, $|a_1|^2$ is symmetric around the $k_{xy} = 0$. Note that all plots are visualized on the same color scale, in the full accessible photoemission horizon.

occurring Floquet engineering might be observed in these experiments. Thus, in general, the sideband amplitude $|a_1|^2$ can contain contributions from Floquet and LAPE processes that we describe with the β and α parameters, respectively. Following the notation of Park [17], the overall sideband amplitude is then given with

$$|a_1|^2 \sim \frac{1}{4}(\beta - \alpha)^2, \quad (2)$$

which intrinsically contains scattering amplitude between both processes. For LAPE, electromagnetic dressing occurs in the photoemission continuum; the free electron final states can be described by Volkov states. In an electron scattering description [17,24,25], the LAPE parameter of the first-order sideband can be calculated with

$$\alpha \sim \left(\frac{e}{m_e \omega_{IR}^2} (E_{xy} k_{xy} \cos(\theta_k - \theta_E) + E_z k_z) \right), \quad (3)$$

as we detail in the Supplemental Material [18]; the in-plane electric field and momentum is written in polar coordinates, as labeled in Fig. 2. ω_{IR} is the driving light frequency, and m_e and e the electron mass and charge.

Before considering the contribution of the Floquet parameter β to the sideband amplitude, we first calculate the expected momentum fingerprints of LAPE sidebands for p - and s -polarized driving light based on Eqs. (2) ($\beta = 0$) and (3) [Figs. 3(a) and 3(b)]. Clearly, the in-plane momentum resolved sideband amplitude $|a_1|^2$ shows distinct azimuthal asymmetries that become more prominent with increasing k_{xy} , where the contribution of the term $\approx E_{xy} k_{xy}$ in Eq. (3) becomes comparable to the out-of-plane component $E_z k_z$. Importantly, we can directly see that LAPE sidebands should

also appear in the case of s -polarized driving. This stands in contrast to typical expectations in experiments that are performed close to the $\bar{\Gamma}$ point, where especially LAPE sidebands are not expected as k_{xy} is considered negligibly small [7].

Based on these momentum fingerprints originating from LAPE, we turn back to the experimental results obtained on Au(111). Figure 4 shows selected (k_x, k_y) momentum maps of the three-dimensional momentum microscopy data sets. Centered at the $\bar{\Gamma}$ point, the occupied part of the SS band is resolved for energies close to the Fermi level (top row). At larger k_x and k_y , the full hexagonal structure of the sp -band transition within the first and the second surface Brillouin zone are resolved. In the two-color experiment with p -polarized driving light, replica sideband structures of the SS band and the sp band 1.2 eV above the original structures are seen [Fig. 4(a), bottom left]. In the following, we will further evaluate the sideband intensities throughout the full measured 3D data set.

First, we systematically vary the polarization angle Φ of the driving laser field from p to s polarization, keeping all other parameters fixed. The in-plane momentum-integrated photoemission yield of the first-order sideband, $I_1(k_{xy}, \theta_k, E - E_F \approx +1.1 \text{ eV})$, is shown in Fig. 4(b). The intensity of the IR driving-induced sideband features drops systematically when the out-of-plane field component is reduced by rotating to overall s polarization. The associated momentum maps for p - and s -polarized driving light are shown in Fig. 4(a), bottom left and right. Strikingly, no distinct photoemission spectral features of the sidebands are resolved for s -polarized driving light within our noise level (which is slightly increased due to photoemission with residual light of a neighboring harmonic with $\hbar\omega = 31.4 \text{ eV}$, see Refs. [18,19]). Based on the calculations shown in Fig. 3, this observation is unexpected at first. For $k_{xy} > 2 \text{ \AA}^{-1}$ and $\Theta_k = 0^\circ$ and 180° , i.e., close to the edge of the photoemission horizon and perpendicular to the plane of incidence of the driving light, sideband intensities should be resolved.

This observation can be understood, however, when taking screening of the IR electromagnetic field in front of the high-electron density Au(111) crystal into account. At the metallic surface, in-plane electric field components with driving frequencies below the plasmon frequency are reflected with near unity; the local in-plane electric field strength within the crystal and in front of the surface is close to zero due to destructive interference of the incoming and outgoing electric field. Thus, at the metallic surface, Eq. (3) must be reconsidered with $E_{xy} = 0$ to

$$\alpha \sim \frac{e}{m_e \omega_{IR}^2} E_z k_z. \quad (4)$$

In the bottom row of Fig. 3, the revised calculations using Eq. (4) are shown. In agreement with experiment, no sideband amplitude is present in s -polarized driving. Following this reasoning, we fit the polarization dependent photoemission yield in Fig. 4(b) with Eq. (4), which nicely describes the experimental results (blue fit). In contrast, if we include in-plane field components, i.e., use Eq. (3), the data are not described to a satisfactory level (grey dashed line).

Having identified the absence of sidebands caused by in-plane field components of the driving laser, we now turn our attention again to p -polarized driving light that contains both

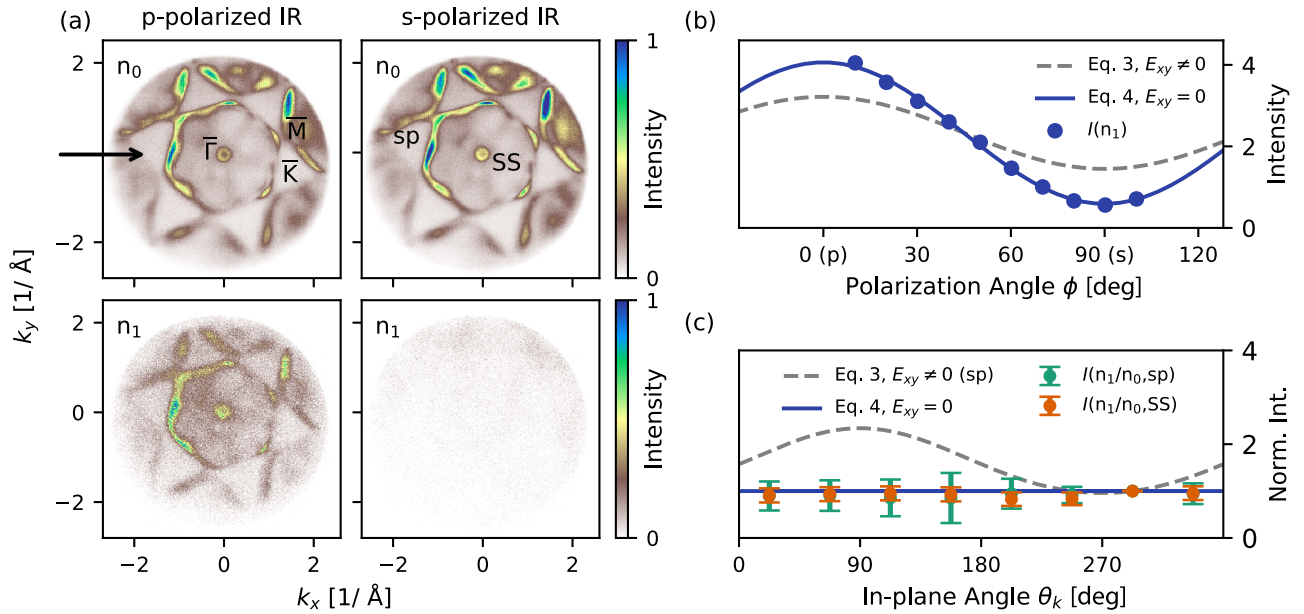


FIG. 4. (a) (k_x, k_y) -resolved momentum maps extracted from the three-dimensional momentum microscopy data obtained with p -polarized EUV light and p - (left column) and s - (right column) polarized IR driving light in temporal overlap. The top row shows momentum maps taken close to the Fermi level that we label as the zero-photon-order sideband n_0 . The high-symmetry points $\bar{\Gamma}$, \bar{K} , \bar{M} , and the Shockley surface band (SS) as well as the sp -band transitions (sp) are indicated. The black arrow represents the direction of light incidence. The bottom row shows the first-order sideband intensity (n_1) around $E - E_F = +1.1$ eV above the Fermi-level for driving with p - (left) and s -polarized (right) IR light. (b) Systematic evaluation of the momentum integrated intensity of the first-order sideband n_1 when rotating from p - to s -polarized light. The data are well approximated with Eq. (4), implicating that the in-plane electric field components are screened ($E_{xy} = 0$). (c) Azimuthal dependence of the sideband intensity of the SS band and the sp -band transition (details on the normalization of the data is provided in the Supplemental Material [18]). The data can be fitted with Eq. (4), indicating that the in-plane component of the electric field is efficiently screened.

in-plane and out-of-plane field components. Since the surface normal component of the electric field (E_z) is not screened in front of the surface, LAPE sidebands must be expected. Indeed, we clearly observe sidebands [Fig. 4(a), bottom left] and now analyze our experimental data to verify either the asymmetric or symmetric intensity fingerprint as shown in Fig. 3(a) or 3(c).

To do so, we plot the expected calculated sideband intensity as a function of azimuthal in-plane angle in Fig. 4(c), which results in an angle-dependent oscillation for the asymmetric case [gray dashed line, corresponding to Fig. 3(a)] and angle-independent intensities for the symmetric case [blue line, corresponding to Fig. 3(c)]. In comparison, the measured relative sideband intensity $I(n_1/n_0)$ of the SS band and the sp transition as a function of azimuthal in-plane angle θ_k are shown as orange and green dots, respectively. Clearly, for both cases, $I(n_1/n_0)$ is not modulated with θ_k (for analysis details see Supplemental Material [18]). For the SS band located at the $\bar{\Gamma}$ point, this is expected as $k_{xy} \approx 0.15 \text{ \AA}^{-1}$ and thus negligible small; Eqs. (3) and (4) would yield similar sideband intensities even with contributions from $E_{xy} \neq 0$. However, the sp -band transition is probed at $k_{xy} \approx 1 \text{ \AA}^{-1}$, and is still not modulated with θ_k . Thus, also under p -polarized driving, we can exclude the predicted momentum asymmetry as shown in Fig. 3(a). Note that an alternative approach for this analysis is a plot of $I(n_1/n_0)$ as a function of k_{xy} (or k_z), which is shown in the Supplemental Material [18], and yields the same result. In consequence, we conclude that, because of

screening, the in-plane electric field components do not contribute to the electromagnetic dressing of the energy spectrum of the metallic surface at high momenta.

Up to now, we have identified two major conclusions. (a) From the calculations [see Fig. 3(b)], it is clear that driving with s -polarized light should create LAPE sidebands with increasing intensity towards the photoemission horizon. (b) If the studied material system is highly reflective for the applied driving frequency, like in our case Au(111) for IR light, the in-plane electric field components are effectively screened in the bulk and in front of the surface; only surface normal field components can lead to the formation of sidebands. Concerning (a), this observation is rather crucial when searching for light-engineered band structures at the edges of the surface Brillouin zone, for example, on graphene and other two-dimensional materials [12,13]: also in case of s -polarized excitation, contributions of LAPE have to be considered.

The open question is whether we can identify Floquet-Bloch contributions to the measured sideband yield in the two-color photoemission data obtained on Au(111). Therefore it is insightful to calculate β and thus the expected momentum fingerprint of the Floquet sideband amplitude. In the Supplemental Material [18], we approximate the form of β , which depends on the initial state momentum dispersion, for the two-dimensional, parabolic surface band (the SS band) and a bulk band transition with a more complex dispersion relation (the sp band transition). In addition, we consider the contribution

of the interference term ($2\beta\alpha$) to $|a_1|^2$ [cf. Eq. (2)], and find an interesting result: in the case of perfectly parabolic bands, interference between Floquet-Bloch and LAPE bands can induce complete destructive interference, i.e., no sidebands would be observable in photoemission.

However, in the case of Au(111), we argue that the Floquet contribution is in any case negligible, and the measured photoemission yield of the sidebands in Fig. 4(a) is caused by LAPE electrons only, as can be understood by considering screening of the driving electromagnetic field at the metallic surface. First, when considering the in-plane field components, like discussed above for LAPE, no Floquet-Bloch sideband amplitude can be expected as $E_{xy} \approx 0$ due to screening. Importantly, this statement is independent of the explicit form of the β parameter, and thus true for all initial states, independent on their momentum dispersion. Second, for electromagnetic dressing with the out-of-plane field component (E_z), the situation is slightly more complex. Both, in front of the surface and in the bulk material, E_z is finite and can thus couple to the k_z component of the initial (Floquet) and the final state (LAPE); the relative strength of the Floquet contribution will then depend on the explicit dispersion of the initial state. Here, we neglect the contribution of the initial state dispersion and only estimate the relative strength of E_z as follows: LAPE is considered to occur close to the crystal, where the surface can act as a sink for momentum conservation in the light-dressing process. In contrast, Floquet-Bloch bands would be created within the bulk material; the electric field has to penetrate into the crystal. In the simplest approach, considering an abrupt metal-vacuum interface that could be described via Fresnel equations, the surface normal field component discontinuously drops at the surface barrier. With the dielectric function of gold [26] and 1.2 eV driving light, we estimate that E_z in the bulk material drops to 2% of its value at the surface. This estimation clearly illustrates that the measured sideband yield in p -polarized driving is dominated by LAPE physics. In addition, it exemplifies how critical the screening capabilities of the material have to be considered, if photoemission band mapping is the method of choice for the investigation and identification of light-engineered electronic band structures. We want to emphasize, however, that a light-induced coherent manipulation of the electronic band structure from a metal surface is possible and also has recently been observed using interferometric photoemission techniques [9].

In conclusion, we present a systematic evaluation of the electromagnetic dressing of the electron energy spectrum at high in-plane momenta, i.e., within the full measured photoemission horizon. In contrast to photoemission experiments focusing on features close to the $\bar{\Gamma}$ point ($k_{xy} \approx 0 \text{ \AA}^{-1}$) [7,15,16], for k_{xy} near the photoemission horizon, the in-plane electric field components E_{xy} can, in principle, induce light-dressing of free electron states, i.e. LAPE. However, our analysis shows that not the external electric field strength defines the dressing response, but that the local electric field strength at the crystal has to be considered. Thus, depending on the frequency dependent dielectric tensor, sideband yield can be largely suppressed (and potentially enhanced) in the two-color photoemission experiment.

Our analysis further shows that the distinct separation of Floquet-Bloch and LAPE contributions in a two-color photoemission experiment is challenging. We believe that from modeling of the expected momentum fingerprints for bands with specific initial state momentum dispersions, such as done for two-dimensional linear bands in Refs. [7,17], and carried out for parabolic bands in the Supplemental Material [18], further insight can be gained. Here, especially for the case of 3D dispersive bulk bands, further theoretical work is needed.

Beyond the macroscopic material properties that define the local electric field strength that can potentially build up Floquet-Bloch (and LAPE) sidebands, further theory efforts suggest that also the time scale of decoherence of the optical excitation [27–29], and the pulse duration of the driving field in relation to the optical cycle duration [13,30] can hinder the creation of light-engineered band structures, even so sufficient electric field strength is available for efficient dressing. Based on our results and those predictions, we speculate that for the on-demand creation and detection of light-engineered band structures, one thus first has to consider the macroscopic material properties, and second choose driving conditions that guarantee a minimum phase space into which energy can dissipate.

This work was funded by the Deutsche Forschungsgemeinschaft (DFG, German Research Foundation) 217133147/SFB 1073, projects B07 and B03. M.R. and G.S.M.J. acknowledge funding by the Alexander von Humboldt Foundation. S.S. acknowledges the Dorothea Schlözer Postdoctoral Program for Women.

-
- [1] D. N. Basov, R. D. Averitt, and D. Hsieh, *Nat. Mater.* **16**, 1077 (2017).
 - [2] T. Oka and S. Kitamura, *Annu. Rev. Condens. Matter Phys.* **10**, 387 (2019).
 - [3] M. S. Rudner and N. H. Lindner, *Nat. Rev. Phys.* **2**, 229 (2020).
 - [4] O. D. Mücke, T. Tritschler, M. Wegener, U. Morgner, and F. X. Kärtner, *Phys. Rev. Lett.* **87**, 057401 (2001).
 - [5] Y. H. Wang, H. Steinberg, P. Jarillo-Herrero, and N. Gedik, *Science* **342**, 453 (2013).
 - [6] E. J. Sie, J. W. McIver, Y.-H. Lee, L. Fu, J. Kong, and N. Gedik, *Nat. Mater.* **14**, 290 (2014).
 - [7] F. Mahmood, C.-K. Chan, Z. Alpichshev, D. Gardner, Y. Lee, P. A. Lee, and N. Gedik, *Nat. Phys.* **12**, 306 (2016).
 - [8] S. Aeschlimann, Ultrafast quasiparticle dynamics in graphene and 2D heterostructures, Ph.D. thesis, University of Hamburg, 2018.
 - [9] M. Reutzler, A. Li, Z. Wang, and H. Petek, *Nat. Commun.* **11**, 2230 (2020).
 - [10] J. W. McIver, B. Schulte, F. U. Stein, T. Matsuyama, G. Jotzu, G. Meier, and A. Cavalleri, *Nat. Phys.* **16**, 38 (2020).
 - [11] N. H. Lindner, G. Refael, and V. Galitski, *Nat. Phys.* **7**, 490 (2011).

- [12] M. A. Sentef, M. Claassen, A. F. Kemper, B. Moritz, T. Oka, J. K. Freericks, and T. P. Devereaux, *Nat. Commun.* **6**, 7047 (2015).
- [13] U. De Giovannini, H. Hübener, and A. Rubio, *Nano Lett.* **16**, 7993 (2016).
- [14] F. Liu, M. E. Ziffer, K. R. Hansen, J. Wang, and X. Zhu, *Phys. Rev. Lett.* **122**, 246803 (2019).
- [15] L. Miaja-Avila, C. Lei, M. Aeschlimann, J. L. Gland, M. M. Murnane, H. C. Kapteyn, and G. Saathoff, *Phys. Rev. Lett.* **97**, 113604 (2006).
- [16] G. Saathoff, L. Miaja-Avila, M. Aeschlimann, M. M. Murnane, and H. C. Kapteyn, *Phys. Rev. A* **77**, 022903 (2008).
- [17] S. T. Park, *Phys. Rev. A* **90**, 013420 (2014).
- [18] See Supplemental Material at <http://link.aps.org/supplemental/10.1103/PhysRevB.102.161403> for a description of the experimental setup, data analysis, and theoretical modeling.
- [19] M. Keunecke, C. Möller, D. Schmitt, H. Nolte, G. S. M. Jansen, M. Reutzler, M. Gutberlet, G. Halasi, D. Steil, S. Steil, and S. Mathias, *Rev. Sci. Instrum.* **91**, 063905 (2020).
- [20] K. Medjanik, O. Fedchenko, S. Chernov, D. Kutnyakhov, M. Ellguth, A. Oelsner, B. Schönhense, T. R. F. Peixoto, P. Lutz, C.-H. Min, F. Reinert, S. Däster, Y. Acremann, J. Viehhaus, W. Wurth, H. J. Elmers, and G. Schönhense, *Nat. Mater.* **16**, 615 (2017).
- [21] G. S. M. Jansen, M. Keunecke, M. Düvel, C. Möller, D. Schmitt, W. Bennecke, F. J. S. Kappert, D. Steil, D. R. Luke, S. Steil, and S. Mathias, *New J. Phys.* **22**, 063012 (2020).
- [22] B. Yan, B. Stadtmüller, N. Haag, S. Jakobs, J. Seidel, D. Jungkenn, S. Mathias, M. Cinchetti, M. Aeschlimann, and C. Felser, *Nat. Commun.* **6**, 10167 (2015).
- [23] M. Reutzler, A. Li, and H. Petek, *Phys. Rev. B* **101**, 075409 (2020).
- [24] L. B. Madsen, *Am. J. Phys.* **73**, 57 (2005).
- [25] J. C. Baggesen and L. B. Madsen, *Phys. Rev. A* **78**, 032903 (2008).
- [26] R. L. Olmon, B. Slovick, T. W. Johnson, D. Shelton, S.-H. Oh, G. D. Boreman, and M. B. Raschke, *Phys. Rev. B* **86**, 235147 (2012).
- [27] E. Kandelaki and M. S. Rudner, *Phys. Rev. Lett.* **121**, 036801 (2018).
- [28] S. A. Sato, U. De Giovannini, S. Aeschlimann, I. Gierz, H. Huebener, and A. Rubio, *J. Phys. B: At. Mol. Opt. Phys.* (2020), doi: [10.1088/1361-6455/abb127](https://doi.org/10.1088/1361-6455/abb127).
- [29] M. Schüler, U. D. Giovannini, H. Hübener, A. Rubio, M. A. Sentef, T. P. Devereaux, and P. Werner, [arXiv:2003.11621](https://arxiv.org/abs/2003.11621).
- [30] M. H. Kalthoff, G. S. Uhrig, and J. K. Freericks, *Phys. Rev. B* **98**, 035138 (2018).